

# Surface Oxygen Atom as a Cooperative Ligand in Pd Nanoparticle Catalysis for Selective Hydration of Nitriles to Amides in Water: Experimental and Theoretical Studies

Ken-ichi Shimizu,<sup>\*,†</sup> Takahiro Kubo,<sup>‡</sup> Atsushi Satsuma,<sup>‡</sup> Takashi Kamachi,<sup>§</sup> and Kazunari Yoshizawa<sup>§</sup>

<sup>†</sup>Catalysis Research Center, Hokkaido University, N-21, W-10, Sapporo 001-0021, Japan

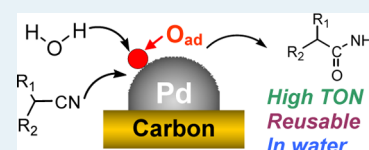
<sup>‡</sup>Department of Molecular Design and Engineering, Graduate School of Engineering, Nagoya University, Nagoya 464-8603, Japan

<sup>§</sup>Institute for Materials Chemistry and Engineering, Kyushu University, Fukuoka 819-0395, Japan

## Supporting Information

**ABSTRACT:** On the basis of an insight in surface science that Pd surfaces partially covered with oxygen adatoms ( $O_{ad}$ ) show higher reactivity for water dissociation than clean Pd surfaces, we studied the effect of  $O_{ad}$  on the activity of carbon-supported palladium metal nanoparticle catalysts (Pd/C) for the selective hydration of nitriles to amides in water. A series of Pd/C with the same Pd loading (5 wt %) and a similar particle size (5.3–6.5 nm) but with different surface coverage of  $O_{ad}$  were prepared and characterized by various spectroscopic methods. The freshly  $H_2$ -reduced Pd/C shows no catalytic activity for hydration of acetonitrile, indicating that clean Pd metal surfaces are inactive. Air exposure of this catalyst under ambient conditions results in the formation of Pd metal NPs partially covered with  $O_{ad}$ , which act as effective and recyclable heterogeneous catalysts for selective hydration of various nitriles to the corresponding amides. Theoretical studies based on density functional theory calculations clarified a cooperative mechanism between metallic Pd and  $O_{ad}$ , in which  $O_{ad}$  as a Brønsted base site plays an important role in the dissociation of water via hydrogen bonding, and the mechanism is verified by kinetic results (activation energy,  $H_2O/D_2O$  kinetic isotope effect, Hammett slope). The mechanistic finding demonstrates a new design strategy of metal nanoparticle catalysts based on a molecular-level understanding of catalysis on oxygen-adsorbed metal surfaces.

**KEYWORDS:** bifunctional catalysis, density functional theory, hydration of nitriles, palladium



## INTRODUCTION

Hydration of nitriles to the corresponding amides is an important transformation from both synthetic and industrial viewpoints.<sup>1</sup> The development of new catalysts for the hydration of nitriles under neutral conditions has received considerable attention, and effective homogeneous<sup>2–12</sup> and heterogeneous<sup>13–24</sup> catalysts have been reported. Notably, several excellent catalysts for this reaction are rationally designed by a concept of “bifunctional catalysis”, in which the metal center acts as a Lewis acid, activating the nitrile molecule, and the ligand acts as a Brønsted base, generating the nucleophile ( $OH^-$  group) from water.<sup>2–10,14</sup> To date, one of the most active catalysts for the hydration of nitriles is the *cis*- $Ru(acac)_2(PPh_2Py)_2$  complex,<sup>4</sup> whose remarkable reactivity can be due to ligand(pyridine nitrogen)-assisted activation of  $H_2O$  via hydrogen bonding, although the catalyst suffers from a difficulty in catalyst/product separation and need for an organic solvent. To expand synthetic utility of this class of catalysts, a highly active bifunctional solid catalyst should be easily prepared from a commercial precatalyst; however, molecular design of new heterogeneous catalysts for hydration of nitriles is difficult because of a lack of molecular-level understanding of catalysis on solid surfaces.

Fundamental studies of water dissociation on well-defined metal surfaces can provide insight into a rational design of metal nanoparticle (NPs) catalysts for organic reactions using

water. Recently, on the basis of the established fact that oxygen-adsorbed Ag surfaces show higher reactivity for water dissociation than clean Ag surfaces, we have developed supported Ag metal NPs with surface oxygen adatoms ( $O_{ad}$ ) as highly effective heterogeneous catalysts for hydration of nitriles.<sup>20</sup> Experimental and theoretical studies of water adsorption on flat Pd surfaces<sup>25–30</sup> indicate that water dissociation does not occur on clean Pd surfaces but does occur on an oxygen adatom-covered Pd surface, leading to the formation of surface OH species. Recent surface science studies have shown that oxygen atoms on the Au(111) surface act as a basic cocatalyst that promotes various organic reactions at low temperatures.<sup>31,32</sup> Knowing these facts, we assumed that Pd NPs covered with  $O_{ad}$  might be effective for organic reactions involving water dissociation as a critical step. On the basis of this strategy, we have recently found that the carbon-supported Pd NPs covered with  $O_{ad}$  act as highly effective and reusable heterogeneous catalysts for the selective hydration of silanes to silanols in water.<sup>33</sup> We report herein that the same type of catalyst, prepared from a commercial Pd–carbon, acts as an effective and recyclable heterogeneous catalyst for the selective hydration of nitriles to amides. Spectroscopic, kinetic, and

Received: July 29, 2012

Revised: October 9, 2012

Published: October 19, 2012

density functional theory (DFT) calculation studies will clarify the reaction mechanism in which  $O_{ad}$  acts as cooperative ligand in Pd NPs catalysis.

## ■ EXPERIMENTAL SECTION

**General.** Commercially available organic compounds (from Tokyo Chemical Industry or Kishida Chemical) were used without further purification. The GC (Shimadzu GC-14B) and GC/MS (Shimadzu GC/MS-QP2010) analyses were carried out with an Ultra ALLOY capillary column UA<sup>+</sup>-5 (Frontier Laboratories Ltd.) using nitrogen as the carrier gas. <sup>1</sup>H NMR spectra were recorded in CDCl<sub>3</sub> with TMS as an internal standard at ambient temperature on a Varian INOVA-500 operating at 500 MHz or a JEOL JNM-ECX 400 operating at 400 MHz.

**Catalyst Preparation.** Pd-carbon (Pd = 5 wt %) was purchased from Kawaken Fine Chemicals. The catalyst named Pd/C-500H was prepared by reducing a commercial Pd-carbon under a flow of 100% H<sub>2</sub> (flow rate = 60 cm<sup>3</sup> min<sup>-1</sup>) at 500 °C for 10 min and cooled to room temperature in a flow of He. The catalyst named Pd/C-500Hox was prepared by exposing Pd/C-500H to air at 25 °C. The catalysts named Pd/C-100Hox and Pd/C-300Hox were prepared in a similar method adopting the temperatures of H<sub>2</sub> reduction of 100 and 300 °C, respectively. Pt/C (Pt = 5 wt %) and Ru/C (Ru = 5 wt %) were purchased from N.E. Chemcat and prepretreated in the same manner as Pd/C-500Hox. Pd black and PdO were purchased from Mitsuwa Chemical.

**Characterization.** The number of oxygen atoms on the catalysts was estimated from the number of CO<sub>2</sub> molecules formed by the reaction of CO + O<sub>ad</sub> = CO<sub>2</sub> at 150 °C. After the in situ formation of the catalyst in a fixed-bed flow reactor (i.d. = 4 mm), the catalyst bed was cooled to 150 °C under a flow of He, then the catalyst was exposed to a flow of 0.4% CO/He at a flow rate of 100 cm<sup>3</sup> min<sup>-1</sup>, and the effluent gas was continuously analyzed by nondispersive infrared CO/CO<sub>2</sub> analyzers (Horiba VIA510). Note that CO<sub>2</sub> might be produced via the water-gas shift reaction (CO + H<sub>2</sub>O = CO<sub>2</sub> + H<sub>2</sub>). In a separate experiment using Pd/C-500Hox, a possible formation of H<sub>2</sub> during the above reaction of O<sub>ad</sub> with CO at 150 °C was checked by online mass spectrometry (BEL Mass, BEL Japan, Inc.). The result showed no formation of H<sub>2</sub>, which confirmed that the determination of the number of O<sub>ad</sub> with our method was adequate.

The Pd K-edge X-ray absorption fine structure (XAFS) measurement was carried out at BL01B1 of SPring-8 (Hyogo, Japan). The storage ring energy was operated at 8 GeV with a typical current of 100 mA. The Fourier transformation of the k<sup>3</sup>-weighted extended X-ray absorption fine structure (EXAFS) oscillation from k space to r space was performed over the range 38–160 nm<sup>-1</sup> to obtain a radial distribution function. The inversely Fourier filtered data were analyzed with a usual curve fitting method in the k range of 38–160 nm<sup>-1</sup> using the empirical phase shift and amplitude functions for Pd–Pd and Pd–O shells extracted from the data for Pd foil and PdO, respectively.

X-ray diffraction (XRD) patterns of the powdered catalysts were recorded with a Rigaku MiniFlex II/AP diffractometer with Cu K $\alpha$  radiation. Average metal particle size was calculated from the half-width of the peak from the XRD pattern using Scherrer equation.

The X-ray photoelectron spectroscopy (XPS) measurements were carried out using a JEOL JPS-900MC with an Al K $\alpha$

anode operated at 20 mA and 10 kV. The oxygen 1s core electron levels in support oxides were recorded. Binding energies were calibrated with respect to C 1s at 285.0 eV.

Transmission electron microscopy (TEM) measurements were carried out using a JEOL JEM-2100F TEM operated at 200 kV.

The adsorption experiment of methylacetate was preformed using a mixture of methylacetate (0.25 mmol) in H<sub>2</sub>O (0.5 mL) and the catalyst (2.5 mg). The mixture was stirred by magnetic stirrer at room temperature in air for 24 h, then the catalyst was removed from the mixture by centrifugation. The amount of methylacetate in the solution was determined by GC using *n*-hexanol as the internal standard, and the number of methylacetate molecules adsorbed on the catalyst was estimated.

**Catalytic Reaction.** A typical procedure for the catalytic reaction is as follows. Pd/C-500Hox (2 mol % Pd with respect to nitrile) was added to a mixture of nitrile (1 mmol) and water (2 g) in a pyrex pressure tube under air, and the mixture was stirred at 95–140 °C. For catalyst screening and kinetic studies, the reaction mixture was analyzed by GC. After the reaction, methanol (cosolvent) and a small amount of *n*-hexanol (internal standard) were added to the reaction mixture, and conversion of the nitrile and yields of products were determined by GC. The products were identified by GC/MS and GC using commercial amides and carboxylic acids as standard compounds.

For the scope and limitation study of Pd/C-500Hox, isolated yields of the amides were determined as follows. After the full conversion of the nitriles, methanol (6 mL) was added to the reaction mixture, and the catalyst was removed by centrifugation, then the solution was evacuated to give the crystalline product, which was identified by <sup>1</sup>H NMR. For the catalytic reaction by the in situ-reduced Pd/C-500H, the reaction mixture was injected to the reduced catalyst inside the glass tube through a rubber stopper. Then, the mixture was stirred at 100 °C under air.

**DFT Calculations.** All calculations were performed with the DMol3 program<sup>34,35</sup> in the Material Studio of Accelrys Inc. The Perdew–Burke–Ernzerhof (PBE) generalized gradient functional was employed for the exchange-correlation energy. The wave functions were expanded in terms of numerical basis sets. We employed the DND basis set (double numerical basis set with the d-type polarization functions) for geometry optimization. Single-point energy calculations were performed with the larger DNP basis set (double numerical basis set with the d-type polarization functions for heavy atoms and the p-type polarization functions for hydrogen atoms). Brillouin zone integrations are performed on a Monkhorst–Pack<sup>36</sup> k-point grid with a k-point spacing of 0.08 Å<sup>-1</sup> unless otherwise noted. The transition state was determined using the linear and quadratic synchronous transit (LST/QST) complete search method.<sup>37</sup> The Pd nanoparticle was modeled by a supercell slab that consists of a 5 × 5 surface unit cell with three atomic (111) surface layers (lattice constants  $a = b = 13.8$  Å). The slab was separated by a vacuum space with a height of 20 Å. The top layer was fully relaxed, whereas the bottom two layers were fixed at the corresponding bulk positions. To confirm the reliability of the selected model, we considered water decomposition with extended models (6 × 6 surface unit cell, 4 surface layers, and k-point spacing of 0.04 Å<sup>-1</sup>). As summarized in Table S1, the differences in calculated energies do not exceed 5 kJ mol<sup>-1</sup>. The lattice constant for bulk Pd was

predicted to be 3.96 Å, which is identical to that from previous DFT calculations<sup>38</sup> and in good agreement with the experimental value of 3.89 Å. The lattice constant is insensitive to the number of k-points (3.97 Å for the k-point spacing of 0.04 and 0.02 Å<sup>-1</sup>), and the electronic energy is well converged for the k-point spacing of <0.05 Å<sup>-1</sup>, as summarized in Supporting Information Table S2.

## RESULTS AND DISCUSSIONS

**Catalyst Characterization.** The catalyst was prepared from a commercial Pd–carbon (named PdO/C). XRD of the as-

**Table 1. Curve-Fitting Analysis of Pd k-Edge EXAFS**

sample	shell	$N^a$	$R$ (Å) <sup>b</sup>	$\sigma$ (Å) <sup>c</sup>	$R_f$ (%) <sup>d</sup>
PdO/C	O	4.3	2.00	0.077	4.3
	Pd	1.5	3.00	0.010	
Pd/C-100Hox	O	0.9	1.99	0.053	0.7
	Pd	6.6	2.73	0.084	
Pd/C-300Hox	O	0.6	1.96	0.051	0.5
	Pd	6.9	2.73	0.078	
Pd/C-500Hox	Pd	6.9	2.74	0.055	0.8

<sup>a</sup>Coordination numbers. <sup>b</sup>Bond distance. <sup>c</sup>Debye–Waller factor. <sup>d</sup>Residual factor.

received Pd–carbon (Figure S1 in the Supporting Information) showed a broad diffraction line due to PdO. The spectral feature of X-ray absorption near-edge structures (XANES) for PdO/C is similar to that for PdO (Supporting Information Figure S2). The EXAFS of PdO/C (Table 1) consists of two shells: a Pd–O shell at bond distance ( $R$ ) of 2.00 Å with coordination number ( $N$ ) of 4.3 and a Pd–O–Pd shell ( $N = 1.5$  at  $R = 3.00$  Å). The TEM result in our previous study<sup>39</sup> showed that the particle sizes of the PdO nanoparticles (NPs) were in a range of 2–5 nm. These results show that the PdO/C catalyst is composed of small PdO NPs.

The catalyst named Pd/C-500H was prepared by H<sub>2</sub> reduction of PdO/C at 500 °C, followed by cooling to room temperature under He without exposing to air. The number of surface metallic Pd atoms on Pd/C-500H was estimated by CO adsorption experiment.<sup>33</sup> On the basis of this value, the average particle size of metallic Pd NPs in Pd/C-500H was estimated to be 6.5 nm (Table 2). Then the catalyst named Pd/C-500Hox

**Table 2. List of Catalysts**

catalysts	Pd (wt %)	$T_{H_2}$ (°C)	$D^b$ (nm)	$[O_{ad}]^c$ (μmol g <sup>-1</sup> )	$[O_{ad}]/[Pd_{surf}]^d$	$[CH_3OAc_{ad}]^e$ (mmol g <sup>-1</sup> )
Pd/C-100Hox	5	100	5.3 ± 0.4	95	1.7	
Pd/C-300Hox	5	300	6.1 ± 0.5	46	0.94	
Pd/C-500Hox	5	500	6.1 ± 0.6	23	0.45	4.28
Pd/C-500H <sup>g</sup>	5	500	6.5 <sup>f</sup>	0.2	0.004	
Pd/TiO <sub>2</sub>	1	500	4.9 <sup>f</sup>			1.71
Pd/Al <sub>2</sub> O <sub>3</sub>	5	500	6.6 <sup>f</sup>	52	0.35	1.28
Pd/ZrO <sub>2</sub>	1	500	3.6 <sup>f</sup>	8.5	0.43	1.20
Pd/CeO <sub>2</sub>	5	500	4.3 <sup>f</sup>			0.76
Pd/SiO <sub>2</sub>	1	500	5.9 <sup>f</sup>	28	2.29	1.85
Pd black	100	300	23 <sup>f</sup>			

<sup>a</sup>Temperatures of reduction in H<sub>2</sub> (10 min). <sup>b</sup>Average metal particle size from TEM. <sup>c</sup>Number of surface oxygen atoms ( $O_{ad}$ ). <sup>d</sup>Ratio of the number of  $O_{ad}$ 's to that of surface Pd atoms estimated from the Pd particle size. <sup>e</sup>Number of methylacetates adsorbed on the catalyst at room temperature in water. Conditions: catalyst = 2.5 mg, methylacetate = 0.25 mmol, H<sub>2</sub>O = 0.5 mL,  $t = 24$  h. <sup>f</sup>Average particle size (nm) of supported metal estimated by CO adsorption. <sup>g</sup>The catalyst was not exposed to air after H<sub>2</sub> reduction at 500 °C.

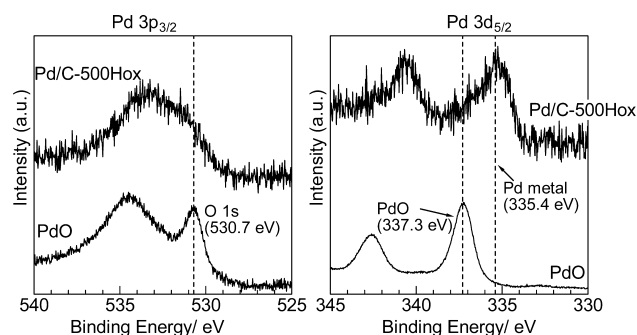
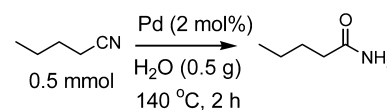


**Figure 1.** XPS spectra of PdO and Pd/C-500Hox.

**Table 3. Hydration of *n*-Pentanenitrile**



entry	catalyst	conv (%)	yield <sup>a</sup> (%)
1	PdO/C <sup>b</sup>	16	16
2	Pd/C-500Hox	71	68
3	PdO	0	0
4	Pd black	9	2
5	Pd/TiO <sub>2</sub>	31	2
6	Pd/Al <sub>2</sub> O <sub>3</sub>	43	28
7	Pd/ZrO <sub>2</sub>	26	10
8	Pd/CeO <sub>2</sub>	44	32
9	Pd/SiO <sub>2</sub>	22	8
10	Pd/MgO	33	17
11	Pt/C	36	24
12	Ru/C	18	18
13	C	0	0

<sup>a</sup>Determined by GC. <sup>b</sup>As-received Pd–carbon.

was prepared by exposing Pd/C-500H to air at room temperature.

The XRD of Pd/C-500Hox (Supporting Information Figure S1) showed the diffraction line at 40.0° due to the (111) of the Pd metal. As shown in our recent study,<sup>33</sup> the average size estimated from TEM analysis is 6.1 ± 0.6 nm, which is nearly consistent with that of Pd/C-500H (6.5 nm). The XANES feature of Pd/C-500Hox is similar to that for Pd foil (Supporting Information Figure S2). The EXAFS of Pd/C-

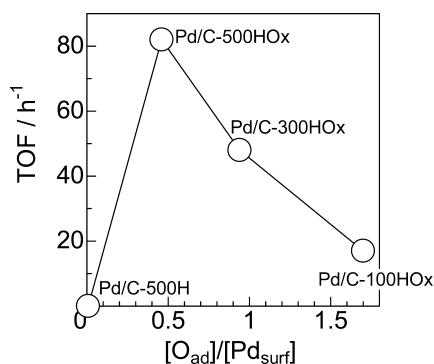


**Figure 2.** TOF based on the number of surface Pd atom vs the ratio of the number of  $O_{ad}$ 's to that of surface Pd atom ( $[O_{ad}]/[Pd_{surf}]$ ) for various Pd/C catalysts. Reaction conditions: acetonitrile (0.5 mmol),  $H_2O$  (0.5 g), Pd/C (2 mol %),  $T = 100\text{ }^\circ\text{C}$ .

**Table 4.** Hydration of Nitriles by Pd/C-500HOx

entry	nitrile	$T/^\circ\text{C}$	yield <sup>a</sup> / %
1		120	89, 90 <sup>b</sup>
2 <sup>c</sup>		120	88
3	$CH_3CN$	115	94
4		135	96
5		135	85
6		135	94
7		130	94
8		135	74
9		135	93
10		135	98
11		135	96
12		95	92
13		125	93

<sup>a</sup>Isolated yield. <sup>b</sup>Fourth reuse. <sup>c</sup>3 mol % Pd,  $t = 36\text{ h}$ .

500HOx (Table 1) consists of a Pd–Pd shell ( $N = 6.9$  at  $R = 2.74\text{ \AA}$ ), which is characteristic of Pd metal. These results show that the bulk structure of the Pd species in Pd/C-500HOx is metallic Pd. The surface structure of this catalyst was investigated by XPS. In the XPS spectrum of Pd/C-500HOx (Figure 1), the Pd  $3d_{5/2}$  peak at 335.4 eV due to metallic Pd and a shoulder peak around 337.3 eV assignable to Pd(II) species were observed. In the O 1s region, there is a weak shoulder at 530.7 eV due to oxygen species of PdO, which

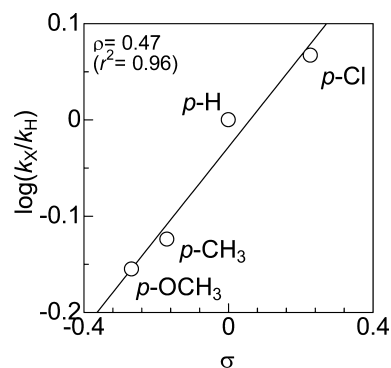


**Figure 3.** Hammett plot for hydration of *p*-substituted benzonitriles. Conditions; *p*-substituted benzonitrile (0.5 mmol),  $H_2O$  (0.5 g), Pd/C-500HOx (2 mol % Pd),  $T = 140\text{ }^\circ\text{C}$ .

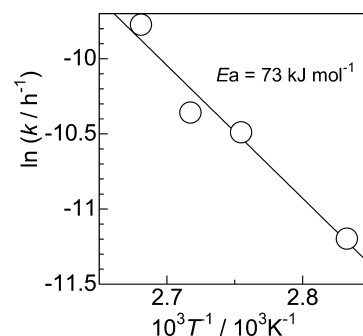


**Figure 4.** Arrhenius plot for the hydration of acetonitrile. Conditions: acetonitrile (0.5 mmol),  $H_2O$  (0.5 g), Pd/C-500HOx (2 mol % Pd).

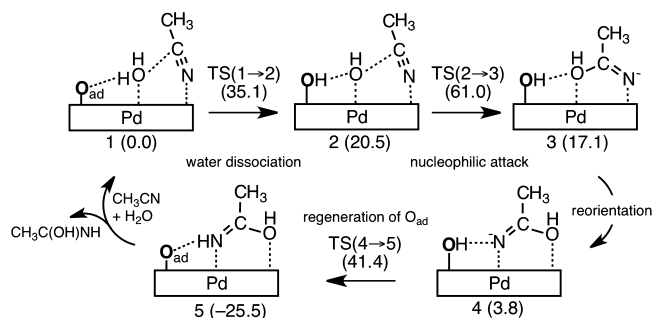


**Figure 5.** Reaction mechanism and computed relative energies (in  $\text{kJ mol}^{-1}$ ) for the hydration of acetonitrile on the Pd(111) surface covered with the surface oxygen atom.

overlaps with a Pd  $3p_{3/2}$  peak at 533.2 eV. These results indicate the presence of surface oxygen atoms ( $O_{ad}$ ) on the metallic Pd NPs.

By changing the  $H_2$  reduction temperature (100 and 300  $^\circ\text{C}$ ), we prepared the samples named Pd/C-100HOx and Pd/C-300HOx, whose average particle sizes from TEM analysis ( $5.3 \pm 0.4$  and  $6.1 \pm 0.5\text{ nm}$ ) were close to that of Pd/C-500HOx (Table 2). XRD, XANES, and EXAFS characterizations of these catalysts showed that the bulk structure of these samples was metallic Pd NPs, and these catalysts did not contain crystalline PdO.<sup>33</sup>

The number of  $O_{ad}$ 's was estimated from the number of  $CO_2$  molecules formed by the reaction of  $CO + O_{ad} = CO_2$  at 150  $^\circ\text{C}$ . The number of  $O_{ad}$ 's decreased with an increase in the  $H_2$  reduction temperature (Table 2). Using the Pd particle size and the number of  $O_{ad}$ 's, the ratio of the number of  $O_{ad}$ 's to that of

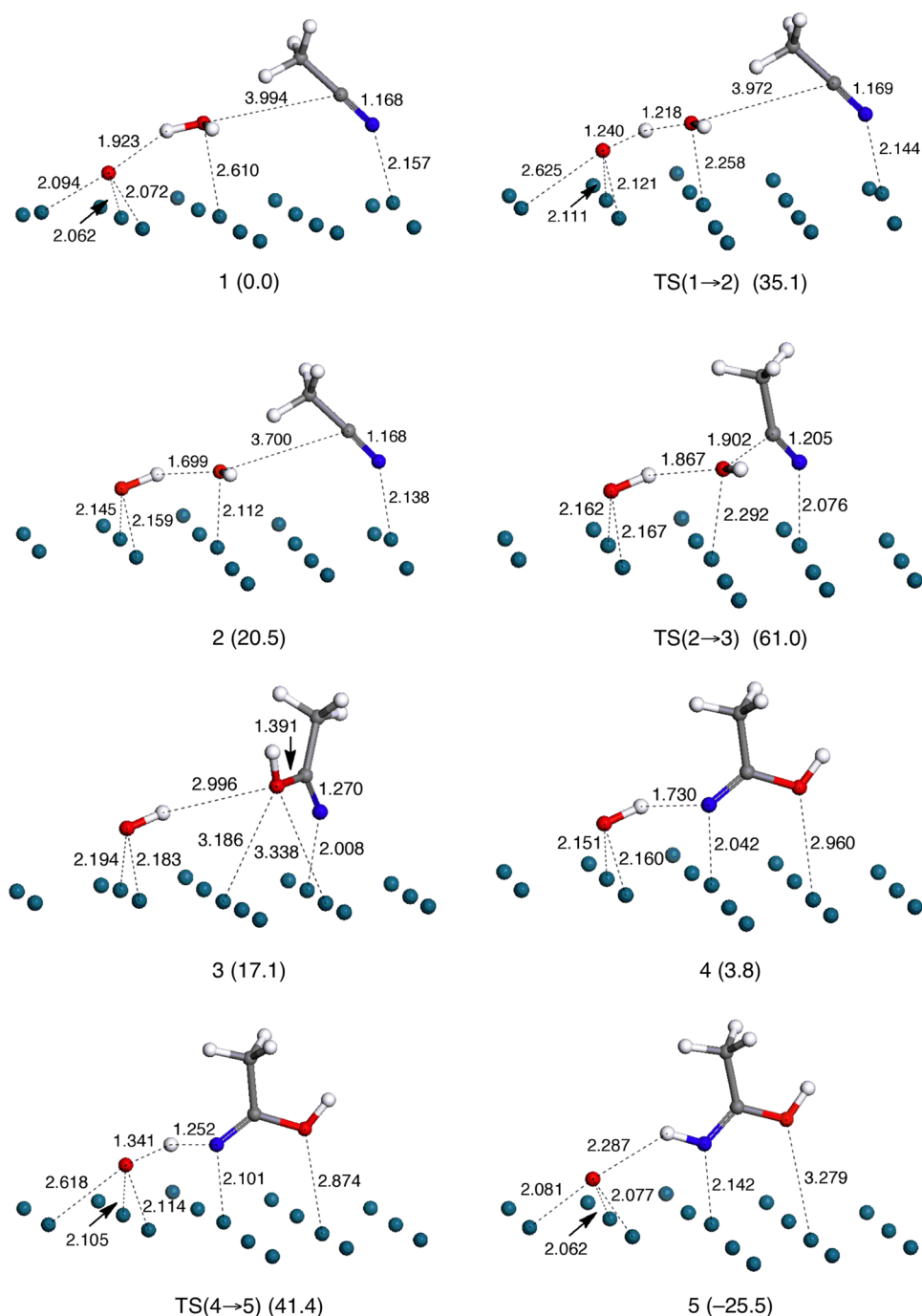


**Figure 6.** Optimized geometries and computed energies for the hydration of acetonitrile on the oxygen atom adsorbed Pd(111) surface. Only the important part is displayed for clarity. Units in Å and kJ mol<sup>-1</sup>. The C, N, O, Pd, and H atoms are colored in gray, blue, red, marine blue, and white, respectively.

surface Pd atoms,  $[O_{ad}]/[Pd_{surf}]$ , was estimated. As shown in Table 2, the  $[O_{ad}]/[Pd_{surf}]$  value, that is, the surface coverage of  $O_{ad}$ 's, decreases with the  $H_2$  reduction temperature. Consequently, a series of Pd NP catalysts with similar Pd size but with different surface coverage of  $O_{ad}$  were prepared. The reason why the Pd NPs reduced at lower temperature have a higher loading of  $O_{ad}$  on their surfaces may be discussed as follows. Reduction at lower temperature may lead to Pd metal NPs with lower degrees of crystallinity, or in other words, larger numbers of surface defects. Because the defects are highly reactive, the low temperature reduction leads to the higher coverage of  $O_{ad}$ .

**Structure–Activity Relationship.** As a model reaction, the selective hydration of acetonitrile to acetamide was studied at 100 °C. Note that oxidation states of Pd surface could change during the reaction, so we measured the initial rate of acetamide formation under the conditions that the acetonitrile conversions were below 15%. The number of surface Pd atoms on the Pd NPs was estimated from the Pd particle size in Table 2. For a series of Pd/C catalysts, the turnover frequency (TOF) per surface Pd atom is plotted as a function of the  $[O_{ad}]/[Pd_{surf}]$  ratio (Figure 2). TOF showed a volcano type dependence on the  $[O_{ad}]/[Pd_{surf}]$  ratio. The Pd/C-500H catalyst, which was used without exposing the prerduced

Table 5. Energies ( $\text{kJ mol}^{-1}$ ) along the C–O Bond Formation Process on the Clean Pd(111) Surface

energy	$d(\text{C}-\text{O})$								
	4.025 <sup>a</sup>	2.500	2.000	1.900	1.800	1.700	1.600	1.550	1.500
	0.0	14.9	59.7	73.9	89.0	103.7	117.8	123.8	130.6

<sup>a</sup>In the following optimized structure, the C, N, O, Pd, and H atoms are colored in gray, blue, red, marine blue, and white, respectively:

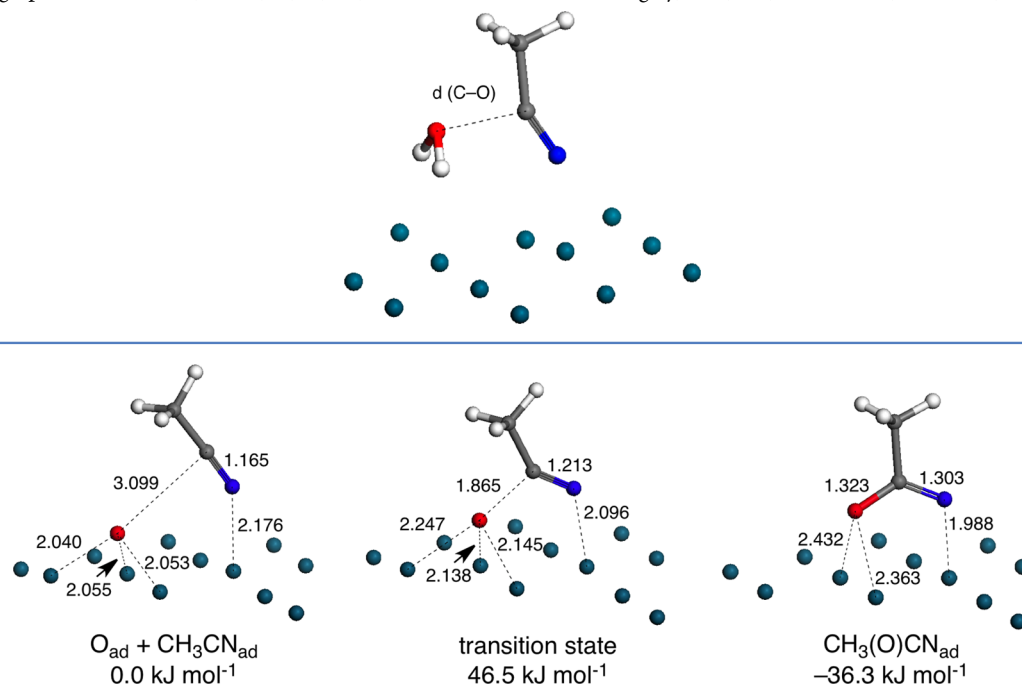


**Figure 7.** Optimized geometries and computed energies for the direct attack of the oxygen atom on the substrate. Only the important part is displayed for clarity. Units in  $\text{\AA}$  and  $\text{kJ mol}^{-1}$ .

catalyst to air, with a negligible value of the  $[\text{O}_{\text{ad}}]/[\text{Pd}_{\text{surf}}]$  ratio showed no activity. After exposing Pd/C-500H to air at room temperature, the catalyst (Pd/C-500Hox) showed a TOF of  $82 \text{ h}^{-1}$ . The Pd/C-500Hox catalyst with a  $[\text{O}_{\text{ad}}]/[\text{Pd}_{\text{surf}}]$  ratio of 0.45 showed the highest TOF, and in a higher coverage region, the TOF decreased with the  $[\text{O}_{\text{ad}}]/[\text{Pd}_{\text{surf}}]$  ratio.

As described in the previous section, Pd/C-100Hox, Pd/C-300Hox, and Pd/C-500Hox do not contain crystalline PdO, but the EXAFS result (Table 1) shows that the number of residual oxygen atoms adjacent to Pd increases with a decrease in the prerduction temperature. Taking into account these structural results, the volcano type dependence of TON on the  $[\text{O}_{\text{ad}}]/[\text{Pd}_{\text{surf}}]$  ratio is discussed as follows. A clean Pd metal surface is nearly inactive for the catalytic hydration of nitriles. The copresence of  $\text{O}_{\text{ad}}$  and vacant  $\text{Pd}^0$  sites leads to high catalytic activity. The decrease in the TOF with the  $\text{O}_{\text{ad}}$  coverage in a high coverage region can be caused by a lower number of  $\text{Pd}^0$  sites available as a catalytic site. The importance of the cooperation between metallic  $\text{Pd}^0$  site and the  $\text{O}_{\text{ad}}$  site in the catalytic cycle will be confirmed by the DFT study.

The activity of various Pd catalysts for the selective hydration of *n*-pentanenitrile to pentanamide is compared in Table 3. Clearly, Pd/C-500Hox showed higher activity than commercial Pd compounds (entries 3, 4), metal oxide-supported Pd catalysts (entries 5–10), and Pt- or Ru-loaded carbon (entries 11, 12). The role of the carbon support in the Pd-catalyzed hydration of nitriles is discussed as follows. As shown in Table 2, the surface oxygen coverages of Pd/ $\text{Al}_2\text{O}_3$  (0.35) and Pd/ $\text{ZrO}_2$  (0.43) are relatively close to that of Pd/C-500Hox (0.45), but the catalytic result in Table 3 shows that the activity of Pd/

C-500Hox is more than two times higher than those of Pd/ $\text{Al}_2\text{O}_3$  and Pd/ $\text{ZrO}_2$ . To compare the hydrophobic nature of the support, we carried out an adsorption experiment of methylacetate in water. The number of methylacetates adsorbed on the catalyst at room temperature in water after 24 h is listed in Table 2. It is found that Pd/C-500Hox shows a larger adsorption capacity than Pd/ $\text{Al}_2\text{O}_3$  and Pd/ $\text{ZrO}_2$ , indicating the higher hydrophobicity of Pd/C-500Hox than the latter catalysts. A comparison of this result with catalytic data (Table 3) suggests that the hydrophobic nature of the carbon support leads to a higher catalytic activity for the hydration of *n*-pentanenitrile in water, possibly because of a larger interaction of the carbon surface with *n*-pentanenitrile than the oxide surface.

**Catalytic Performance.** Next, we examined the catalytic performance of Pd/C-500Hox (2 mol %), as shown in Table 4. Hydration of *n*-pentanenitrile was carried out by Pd/C-500Hox at  $120 \text{ }^\circ\text{C}$  for 24 h (entry 1). After the separation of the catalyst, followed by evaporation of the filtrate, the corresponding amide was obtained with high isolated yield (89%). No byproducts were observed by GC and  $^1\text{H}$  NMR analyses. The TOF based on the total Pd atoms is  $1.8 \text{ h}^{-1}$ , which is an order of magnitude larger than that of Ag/ $\text{SiO}_2$  ( $0.2 \text{ h}^{-1}$  at  $160 \text{ }^\circ\text{C}$ ) reported in our previous study.<sup>20</sup> Then the catalyst was retrieved from the mixture by centrifugation. After washing the removed catalyst with water, followed by drying at  $90 \text{ }^\circ\text{C}$  for 12 h, the catalyst showed a lower amide yield (75%) under the same conditions. Note that the number of  $\text{O}_{\text{ad}}$ 's in the spent catalyst ( $86 \text{ } \mu\text{mol g}^{-1}$ ) was larger than that of the fresh catalyst ( $23 \text{ } \mu\text{mol g}^{-1}$ ). Thus, the observed deactivation can be due to a further

oxidation of the Pd surface during the reaction for 24 h and the subsequent drying treatment. However, after H<sub>2</sub> reduction at 500 °C followed by air exposure at 25 °C, the recovered catalyst was reused at least four times without catalyst deactivation (entry 1). Other aliphatic nitriles (entries 2,3), aromatic nitriles (entries 4–7),  $\alpha,\beta$ -unsaturated nitrile (entry 8), and heteroaromatic nitriles (entries 9–13) were also selectively hydrated to the corresponding amides in good isolated yields (88–98%). Several effective catalytic systems for the selective hydration of in water are already known. The catalytic properties of Pd/C-500Hox for the selective hydration of *n*-hexanenitrile and pyridinenitrile in water are compared with those of previous heterogeneous catalysts in Supporting Information Tables S3 and S4, respectively. To the best of our knowledge, this is among rare catalysts<sup>21</sup> that are effective for both a less reactive aliphatic nitrile (*n*-hexanenitrile) and a highly coordinative nitrile (pyridinenitrile) at relatively low temperatures (95–120 °C) and low catalyst loading (2 mol %).

**Kinetic Studies.** To discuss the reaction mechanism, we carried out kinetic studies using Pd/C-500Hox. First, the kinetic isotope effect (KIE) for the acetonitrile hydration was studied at 100 °C; the initial rate ( $r_{\text{H}}$ ,  $r_{\text{D}}$ ) with H<sub>2</sub>O and D<sub>2</sub>O were measured at the same conversion level (10%). The secondary KIE ( $r_{\text{H}}/r_{\text{D}}$ ) of 1.2 was observed, indicating that H<sub>2</sub>O dissociation is kinetically important, but other steps are kinetically more relevant. Next, we examined the relationship between the relative rates and the Hammett parameter ( $\sigma$ ) for the hydration of *p*-substituted benzonitriles (Figure 3). There is a good linearity between  $\log(k_{\text{X}}/k_{\text{H}})$  and  $\sigma$ , giving a positive slope ( $\rho = 0.47$ ), indicating that a transition state in the rate-limiting step of the catalytic reaction has a negative charge at the  $\alpha$ -carbon atom adjacent to the phenyl group. Considering the KIE of 1.2, the positive  $\rho$  value suggests that the rate-limiting step includes a nucleophilic addition of OH <sup>$\delta^-$</sup>  species to the nitrile carbon atom of nitrile species via a negatively charged transition state. An Arrhenius plot for the acetonitrile hydration (Figure 4) showed the activation energy of 73 kJ mol<sup>-1</sup>.

**DFT Calculation Studies.** On the basis of the above findings, we explored a possible reaction pathway for the hydration of acetonitrile on the Pd(111) surface with an O<sub>ad</sub> species using periodic DFT calculations. Note that the Pd particle size of 6.1 nm in Pd/C-500Hox indicates that a majority of the surface metal atoms are at plane sites. Thus, the Pd nanoparticle is reasonably modeled by the Pd(111) periodic slab. The reaction mechanism and energetics are schematically represented in Figure 5. The optimized structures are shown in Figure 6. The first step (1  $\rightarrow$  2) is water dissociation on the surface, where O<sub>ad</sub> acts as a Brønsted base for the proton abstraction from H<sub>2</sub>O, leading to the formation of two OH groups on the Pd surface. The water molecule and the surface oxygen atom are on the top and 3-fold sites, respectively, in the most favorable coadsorption state of 1. A strong hydrogen bond of 1.923 Å is formed between the water molecule and O<sub>ad</sub> in 1 because O<sub>ad</sub> is negatively charged (-0.65) by the nearest three Pd atoms (+0.21 on average). The acetonitrile molecule is coadsorbed on the top of Pd and is weakly bonded to the oxygen atom of the water molecule; the Pd $\cdots$ N and C $\cdots$ O distances are 2.157 and 3.994 Å, respectively. Then the water molecule is deprotonated by the O<sub>ad</sub> site with an activation energy of 35.1 kJ mol<sup>-1</sup>. The water dissociation process is endothermic by 20.5 kJ mol<sup>-1</sup>. These results are consistent with the previous DFT studies.<sup>25,26</sup> In the absence of O<sub>ad</sub>, the

activation barrier for the water decomposition on a Pd(111) surface is 105 kJ mol<sup>-1</sup>. Thus, the water decomposition is unlikely to occur on the clean Pd surface due to the much higher activation barrier.

We considered a direct attack of the water molecule to the carbon atom of the adsorbed acetonitrile on a clean Pd(111) surface to rule out the possibility that the hydration reaction proceeds without the activation of water molecules by the surface oxygen atom. We scanned the potential-energy surface along the C–O coordinate using partial optimization (Table 5). The potential-energy surface ascends steeply with the decrease in the C–O distance. The relative energy was calculated to be 130.6 kJ mol<sup>-1</sup> (at the C–O distance of 1.500 Å), which is much higher than the experimentally determined activation energy. These computational results support our proposal that the surface oxygen atom is required to produce active OH species on the Pd surface.

The C $\cdots$ O distance between the nitrile carbon atom and the OH group derived from the water molecule is shortened from 3.994 in 1 to 3.700 Å in 2, which indicates that the negatively charged OH group attracts the nitrile carbon atom of the coadsorbed acetonitrile molecule. The nucleophilic attack of the OH species occurs via TS(2  $\rightarrow$  3) to form a C–O bond. In the transition state, the acetonitrile molecule migrates to a neighboring top site, whereas the OH group remains nearly at the initial position. The C $\cdots$ O distance was calculated to be 1.902 Å in the transition state. The activation barrier of the C–O bond formation is 61.0 kJ mol<sup>-1</sup> measured from 1. The calculated activation energy is in good agreement with the experimental value of 73 kJ mol<sup>-1</sup>. It is worth noting that pure DFT methods tend to underestimate barrier heights for chemical reaction.<sup>40</sup> Thus, the calculated barrier is quite reasonable. TS(2 $\rightarrow$ 3) is energetically highest in the reaction pathway, and the overall reaction is exothermic. Thus, the C–O bond formation is the rate-determining step in the reaction, which is consistent with the observed low KIE value of 1.2. The atomic charge of the nitrile nitrogen atom decreases from -0.17 in 2 to -0.37 in 3 upon addition of the negatively charged OH species to the acetonitrile molecule. The N $\cdots$ Pd distance varies from 2.138 Å to 2.008 in the course of the C–O bond formation, which implies that the Pd surface promotes the nucleophilic attack by partially accepting the negative charge on the nitrogen atom. The reorientation of the intermediate (3  $\rightarrow$  4) readily takes place as a result of the Coulombic interaction between the remaining OH group and the negatively charged nitrogen atom, this step being 13.3 kJ mol<sup>-1</sup> exothermic. In the final step (4  $\rightarrow$  5), the nitrogen atom accepts a proton from the OH group with the regeneration of the O<sub>ad</sub> site. This step is exothermic by 29.3 kJ mol<sup>-1</sup>, with an activation energy of 37.6 kJ mol<sup>-1</sup>. Thus, the O<sub>ad</sub> site is efficiently regenerated on the Pd surface in the catalytic cycle, which would be a key mechanistic feature of the catalyst for the high TON. The produced hydrated nitrile species is released into the solvent and is easily converted into acetamide with the aid of a bridging water molecule (Figure S3).

For the purpose of comparison, we investigated the direct attack of the surface oxygen atom to the coadsorbed acetonitrile molecule in the absence of water molecules, as shown in Figure 7. The direct attack is an undesired dead-end reaction because the surface oxygen atoms, which are responsible for the water activation, are consumed. Our DFT calculations show that the direct attack is exothermic by 36.3 kJ mol<sup>-1</sup>, with an activation energy of 46.5 kJ mol<sup>-1</sup>. This barrier is 11.4 kJ mol<sup>-1</sup> higher

than that for the water decomposition, indicating that the water decomposition is more facile than the direct attack. Furthermore, the coadsorbed water molecule would suppress the undesired reaction because the strong hydrogen bond between the water molecule and the surface oxygen atom does not allow direct contact of acetonitrile with the surface oxygen atom.

Summarizing the theoretical and experimental (kinetic) studies on the acetonitrile hydration by the Pd NPs catalyst, a catalytic cycle was clarified as shown in Figure 5. A key feature is a bifunctional mechanism between metallic Pd and  $O_{ad}$ , where  $O_{ad}$  as a Brønsted base site plays an important role in the dissociation of water via hydrogen bonding. This model is basically consistent with a well-known concept of “bifunctional catalysis”, in which the metal center acts as a Lewis acid, activating the nitrile molecule, and the ligand acts as a Brønsted base, generating the nucleophile ( $OH^-$  group) from water.<sup>2–10,14</sup> An important insight from our conclusion is that the highly active bifunctional heterogeneous catalyst can be easily prepared from a commercial precatalyst by simply adding the oxygen atoms on the surface of the Pd metal NPs.

## CONCLUSION

On the basis of the well established fact in surface science that oxygen-adsorbed Pd surfaces show higher reactivity for water dissociation than clean Pd surfaces, we have found that the carbon-supported Pd NPs partially covered with  $O_{ad}$  act as a highly effective and reusable heterogeneous catalyst for the selective hydration of nitriles to amides. Fundamental studies clarified a cooperative mechanism between metallic Pd and  $O_{ad}$ , where  $O_{ad}$  as a Brønsted base site plays an important role in the dissociation of water via hydrogen bonding. These findings demonstrate that a surface-science-driven strategy is useful to design new metal NPs catalyst for green organic reactions involving water dissociation as a critical step.

## ASSOCIATED CONTENT

### Supporting Information

Additional information as noted in text. This material is available free of charge via the Internet at <http://pubs.acs.org>.

## AUTHOR INFORMATION

### Corresponding Author

\*Fax: +81-11-706-9163. E-mail: [kshimizu@cat.hokudai.ac.jp](mailto:kshimizu@cat.hokudai.ac.jp).

### Notes

The authors declare no competing financial interest.

## ACKNOWLEDGMENTS

This work was supported by Grants-in-Aid for Scientific Research (20360361, 22245028, 22686075, 24550190) and a program “Elements Strategy Initiative to Form Core Research Center” (since 2012), MEXT, Japan.

## REFERENCES

- (1) March, J. *Advanced Organic Chemistry*, Wiley-Interscience: New York, 1992, 383.
- (2) Ahmed, T. J.; Knapp, S. M. M.; Tyler, D. *Coord. Chem. Rev.* **2011**, *255*, 949.
- (3) Kim, J. H.; Britten, J.; Chin, J. *J. Am. Chem. Soc.* **1993**, *115*, 3618.
- (4) Oshiki, T.; Yamashita, H.; Sawada, K.; Utsunomiya, M.; Takahashi, K.; Takai, K. *Organometallics* **2005**, *24*, 6287.
- (5) García-Álvarez, R.; Díez, J.; Crochet, P.; Cadierno, V. *Organometallics* **2010**, *29*, 3955.

- (6) Yi, C. S.; Zeczycki, T. N.; Lindeman, S. V. *Organometallics* **2008**, *27*, 2030.
- (7) Fung, W. K.; Huang, X.; Man, M. L.; Ng, S. M.; Hung, M. Y.; Lin, Z.; Lau, C. P. *J. Am. Chem. Soc.* **2003**, *125*, 11539.
- (8) Leung, C. W.; Zheng, W.; Zhou, Z.; Lin, Z.; Lau, C. P. *Organometallics* **2008**, *27*, 4957.
- (9) Hirano, T.; Uehara, K.; Kamata, K.; Mizuno, N. *J. Am. Chem. Soc.* **2012**, *134*, 6425.
- (10) García-Álvarez, R.; Díez, J.; Crochet, P.; Cadierno, V. *Organometallics* **2011**, *30*, 5442.
- (11) Goto, A.; Endo, K.; Saito, S. *Angew. Chem., Int. Ed.* **2008**, *47*, 3607.
- (12) Ishizuka, A.; Nakazaki, Y.; Oshiki, T. *Chem. Lett.* **2009**, *38*, 360.
- (13) Yamaguchi, K.; Mizugaki, T.; Ebitani, K.; Kaneda, K. *Chem. Commun.* **2001**, *37*, 461.
- (14) Yamaguchi, K.; Matsushita, M.; Mizuno, N. *Angew. Chem., Int. Ed.* **2004**, *43*, 1576.
- (15) Bazi, F.; El Badaoui, H.; Tamani, S.; Sokori, S.; Solhy, A.; Macquarrie, D. J.; Sebti, S. *Appl. Catal., A* **2006**, *301*, 211.
- (16) Mitsudome, T.; Mikami, Y.; Mori, H.; Arita, S.; Mizugaki, T.; Jitsukawa, K.; Kaneda, K. *Chem. Commun.* **2009**, *45*, 3258.
- (17) Polshettiwar, V.; Varma, R. S. *Chem.—Eur. J.* **2009**, *15*, 1582.
- (18) Miura, H.; Sugiyama, K.; Kawakami, S.; Aoyama, T.; Matsuda, T. *Chem. Lett.* **1982**, *11*, 183.
- (19) Tamura, M.; Wakasugi, H.; Shimizu, K.; Satsuma, A. *Chem.—Eur. J.* **2011**, *17*, 11428.
- (20) Shimizu, K.; Imaiida, N.; Sawabe, K.; Satsuma, A. *Appl. Catal., A* **2012**, *421–422*, 114.
- (21) Liu, Y.; He, L.; Wang, M.; Cao, Y.; He, H.; Fan, K. *ChemSusChem* **2012**, *5*, 1392.
- (22) García-Garrido, S. E.; Francos, J.; Cadierno, V.; Basset, J.-M.; Polshettiwar, V. *ChemSusChem* **2011**, *4*, 104.
- (23) Lee, W.; Frost, B. J. *Green Chem.* **2012**, *14*, 62.
- (24) Nasir Baig, R. B.; Varma, R. S. *Chem. Commun.* **2012**, *48*, 6220.
- (25) Cao, Y.; Chen, Z.-X. *Surf. Sci.* **2006**, *600*, 4572.
- (26) Cao, Y.; Chen, Z.-X. *Phys. Chem. Chem. Phys.* **2007**, *9*, 739.
- (27) Shavorskiy, A.; Gladys, M. J.; Held, G. *Phys. Chem. Chem. Phys.* **2008**, *10*, 6150.
- (28) Pan, M.; Hoang, S.; Mullins, C. B. *Catal. Today* **2011**, *160*, 198.
- (29) Zhu, X.; White, J.; Wolf, W.; Hasselbrink, E.; Ertl, G. *J. Phys. Chem.* **1991**, *95*, 8393.
- (30) Gladys, M. J.; El Zein, A. A.; Mikkelsen, A.; Andersen, J. N.; Held, G. *Surf. Sci.* **2008**, *602*, 3540.
- (31) Gong, J. L.; Mullins, C. B. *Acc. Chem. Res.* **2009**, *42*, 1063.
- (32) Xu, B.; Zhou, L.; Madix, R. J.; Friend, C. M. *Angew. Chem., Int. Ed.* **2010**, *49*, 343.
- (33) Shimizu, K.; Kubo, T.; Satsuma, A. *Chem.—Eur. J.* **2012**, *18*, 2226.
- (34) Delley, B. *J. Chem. Phys.* **1990**, *92*, 508.
- (35) Delley, B. *J. Chem. Phys.* **2000**, *113*, 7756.
- (36) Monkhorst, H. J.; Pack, J. D. *Phys. Rev. B.* **1976**, *13*, 5188.
- (37) Govind, N.; Petersen, M.; Fitzgerald, G.; King-Smith, D.; Andzelm, J. *Comput. Mater. Sci.* **2003**, *28*, 250.
- (38) Eichler, A.; Mittendorfer, F.; Hafner, J. *Phys. Rev. B* **2000**, *62*, 4744.
- (39) Shimizu, K.; Koizumi, S.; Hatamachi, T.; Yoshida, H.; Komai, S.; Kodama, T.; Kitayama, Y. *J. Catal.* **2004**, *228*, 141.
- (40) Zhao, Y.; González-García, N.; Truhlar, D. G. *J. Phys. Chem. A* **2005**, *109*, 2012.